INTERNATIONAL JOURNAL FOR NUMERICAL METHODS IN FLUIDS
Int. J. Numer. Meth. Fluids 2004; **45**:43–51 (DOI: 10.1002/fld.663)

On the application of slip boundary condition on curved boundaries

Marek Behr*,†

Lehrstuhl für Numerische Mechanik, Fakultät für Maschinenwesen, Technische Universität München, D-85747 Garching, Germany

SUMMARY

Hydrodynamic simulations of sloshing phenomena often involve the application of slip boundary condition at the wetted surfaces. If these surfaces are curved, the ambiguous nature of the normal vector in the discretized problem can interfere with the application of such a boundary condition. Even the use of consistent normal vectors, preferred from the point of view of conservation, does not assure good approximation of the continuum slip condition in the discrete problem, and non-physical recirculating flow fields may be observed. As a remedy, we consider the Navier slip condition, and more successfully, the so-called BC-free boundary condition. Copyright © 2004 John Wiley & Sons, Ltd.

KEY WORDS: slip boundary condition; outflow boundary condition; curved boundaries; free-surface flows

1. INTRODUCTION

Fluid flow simulations involving deforming domains in general, and free-surface flow simulations in particular, pose unique modelling challenges. Interface-tracking approach, in which the computational mesh follows the deformation of the domain, and its boundaries always coincide with the boundaries of the fluid, offers sharp resolution of the interface at modest computational cost and is therefore useful in situations where the deformation is significant but not dramatic. However, the need to track the free surface via explicit enforcement of the kinematic conditions (e.g. no-flux), and the need to adapt the computational mesh in response to the free-surface movement are some of the complications inherent in the interface-tracking approach considered here. Free and moving boundary simulations have been the subject of intense study—see e.g. References [1–5] and others.

In addition to the need to enforce the kinematic conditions at the free surface boundary, hydrodynamic simulations routinely require that a paradox of moving contact line at a

*Correspondence to: M. Behr, Lehrstuhl für Numerische Mechanik, Fakultät für Maschinenwesen, Technische Universität München, D-85747 Garching, Germany.
†E-mail: behr@lnm.mw.tum.de

Contract/grant sponsor: National Science Foundation; contract/grant number: CTS-ITR-0312764

Received 1 April 2003
Revised 24 September 2003

no-slip wetted surface be resolved [6]. Slip condition is thus employed, at a minimum, at the portion of wetted surface immediately adjacent to the free surface. Moreover, simulations that involve low-viscosity fluids and large length scales often call for the application of slip boundary condition at the entire wetted surface. Such a condition is straightforward to apply at boundaries that coincide with Cartesian co-ordinate planes, and is also routinely applied at slanted and curved boundaries [7]. If these surfaces are in fact curved, the ambiguous nature of the normal vector in the discretized problem can interfere with the proper representation of full-slip boundary condition. Even the use of consistent normal directions [7], which are most suitable for proper mass and momentum conservation, does not guarantee good approximation of the continuum slip condition in the discrete problem, and non-physical recirculating flow fields are observed in some numerical experiments.

We work in the context of the deformable-spatial-domain/stabilized space–time (DSD/SST) finite element formulation [8, 9], which has been applied to many classes of flow problems involving moving boundaries and interfaces [10]. In space–time methods, the stabilized finite element formulations of the governing equations are written over the space–time domain of the problem. Consequently, changes in the shape of the spatial domain due to the motion of the boundaries and interfaces are taken into account automatically, being reflected in the deformation of space–time elements. This approach has been successfully used to solve sloshing problems [11], flows past a surface-piercing obstacles [12, 13], as well as other classes of deforming-domain problems [14, 15]. In the context of free-surface problems in complex geometries, the DSD/SST formulation must be coupled with a suitable algorithm for the motion of the free surface, such as the standard elevation equation for flows in channels with vertical side walls, or a generalized elevation equation for flows where the side walls may be slanted or curved. Although space–time methods are used here, our discussion of the slip boundary condition is equally applicable to the more traditional ALE approach [16].

In Section 2, we review the governing equations and their stabilized finite element formulation. In Section 3, we focus on the issue of proper application of slip boundary condition in the presence of curved boundaries, and illustrate the problem in Section 4, while also proposing a remedy in the form of BC-free boundary condition. We end with concluding remarks in Section 5.

2. GOVERNING EQUATIONS AND DISCRETIZATION

We consider a viscous, incompressible fluid occupying a time-varying domain $\Omega_t \subset \mathbb{R}^{n_{sd}}$, with boundary Γ_t, where n_{sd} is the number of space dimensions. Velocity $\mathbf{u}(\mathbf{x},t)$ and pressure $p(\mathbf{x},t)$ fields are governed by the incompressible Navier–Stokes equations:

$$\rho(\mathbf{u}_{,t} + \mathbf{u} \cdot \nabla\mathbf{u} - \mathbf{f}) - \nabla \cdot \boldsymbol{\sigma} = \mathbf{0} \quad \text{on } \Omega_t \tag{1}$$

$$\nabla \cdot \mathbf{u} = 0 \quad \text{on } \Omega_t \tag{2}$$

where $\mathbf{f}$ is the body force such as gravity, and the density ρ is assumed to be constant. For a Newtonian fluid, stress tensor $\boldsymbol{\sigma}$ is

$$\boldsymbol{\sigma}(\mathbf{u}, p) = -p\mathbf{I} + 2\mu\boldsymbol{\varepsilon}(\mathbf{u}), \qquad \boldsymbol{\varepsilon}(\mathbf{u}) = \tfrac{1}{2}(\nabla\mathbf{u} + (\nabla\mathbf{u})^{\mathrm{T}}) \tag{3}$$

where μ is the dynamic viscosity. The Dirichlet and Neumann-type boundary conditions are:

$$\mathbf{u} = \boldsymbol{g} \quad \text{on } (\Gamma_t)_{\boldsymbol{g}} \tag{4}$$

$$\mathbf{n} \cdot \boldsymbol{\sigma} = \boldsymbol{h} \quad \text{on } (\Gamma_t)_{\boldsymbol{h}} \tag{5}$$

where $(\Gamma_t)_{\boldsymbol{g}}$ and $(\Gamma_t)_{\boldsymbol{h}}$ are complementary subsets of the boundary Γ_t.

The finite element function spaces for the space–time method are based on the partition of the time interval $(0, T)$ into subintervals $I_n = (t_n, t_{n+1})$, where t_n and t_{n+1} belong to an ordered series of time levels $0 = t_0 < t_1 < \cdots < t_N = T$. Let $\Omega_n = \Omega_{t_n}$ and $\Gamma_n = \Gamma_{t_n}$. We define the space–time slab Q_n as the domain enclosed by the surfaces Ω_n, Ω_{n+1}, and P_n, where P_n is the surface described by the boundary Γ_t as t traverses I_n. As it is the case with Γ_t, surface P_n is decomposed into $(P_n)_{\boldsymbol{g}}$ and $(P_n)_{\boldsymbol{h}}$ with respect to the type of boundary condition (Dirichlet and Neumann) being applied.

After introducing suitable trial solution spaces for the velocity and pressure [11], $(\mathscr{S}^h_{\mathbf{u}})_n$ and $(\mathscr{S}^h_p)_n$, and test function spaces, $(\mathscr{V}^h_{\mathbf{u}})_n$ and $(\mathscr{V}^h_p)_n$, the stabilized space–time formulation of Equations (1) and (2) is written as follows: given $(\mathbf{u}^h)^-_n$, find $\mathbf{u}^h \in (\mathscr{S}^h_{\mathbf{u}})_n$, and $p^h \in (\mathscr{S}^h_p)_n$ such that $\forall \mathbf{w}^h \in (\mathscr{V}^h_{\mathbf{u}})_n$ and $\forall q^h \in (\mathscr{V}^h_p)_n$:

$$\begin{aligned}
&\rho(\mathbf{w}^h, \mathbf{u}^h_{,t} + \mathbf{u}^h \cdot \nabla \mathbf{u}^h - \mathbf{f}^h)_{Q_n} + (\boldsymbol{\varepsilon}(\mathbf{w}^h), \boldsymbol{\sigma}(\mathbf{u}^h, p^h))_{Q_n} \\
&\quad + (q^h, \nabla \cdot \mathbf{u}^h)_{Q_n} + \rho((\mathbf{w}^h)^+_n, (\mathbf{u}^h)^+_n - (\mathbf{u}^h)^-_n)_{\Omega_n} \\
&\quad + \sum_{e=1}^{(n_{\text{el}})_n} \frac{\tau}{\rho}(\rho(\mathbf{w}^h_{,t} + \mathbf{u}^h \cdot \nabla \mathbf{w}^h) - \nabla \cdot \boldsymbol{\sigma}(\mathbf{w}^h, q^h), \\
&\qquad \rho(\mathbf{u}^h_{,t} + \mathbf{u}^h \cdot \nabla \mathbf{u}^h - \mathbf{f}^h) - \nabla \cdot \boldsymbol{\sigma}(\mathbf{u}^h, p^h))_{Q^e_n} = (\mathbf{w}^h, \boldsymbol{h}^h)_{(P_n)_{\boldsymbol{h}}}
\end{aligned} \tag{6}$$

where $(\cdot, \cdot)_\square$ are the appropriate scalar or vector function inner products over domain $\square$, $(\mathbf{u}^h)^\pm_n = \lim_{\varepsilon \to 0} \mathbf{u}(t_n \pm \varepsilon)$, and the parameter τ follows the definition in Reference [11]. In most applications of our method, both velocity and pressure fields are represented using piecewise linear continuous interpolation functions. We draw the reader's attention to the last term in Equation (6), which is a means of imposing tangent normal stresses $\boldsymbol{h}^h$ at a domain boundary, and will be essential in the discussion that follows. Note that $\boldsymbol{h}$ stands for applied traction while superscript h denotes discretized quantities.

The non-linear system given by Equation (6) is solved with the Newton–Raphson method. For deforming-domain free-surface simulations considered here, the governing equations for the flow field are augmented by two additional equations governing the deformation of the mesh—the generalized elevation equation introduced in Reference [13] extended to curved geometries, and the elasticity equation that governs the displacement of the interior mesh nodes in response to boundary movement, described in Reference [17]. The exact form of these equations is not recounted here, as it is not a prerequisite for the discussion that follows.

3. SLIP BOUNDARY CONDITIONS

A slip boundary condition is often employed in hydrodynamic simulations at solid boundaries. Slip condition is a means of circumventing the 'kinematic paradox', as described by Kistler [6], of a moving contact line at a no-slip boundary. A wetting model may be employed as part of the slip condition, as described by Baer *et al.* [5], and the condition itself may be restricted to the small 'slip zone' in the immediate vicinity of the free surface. In the area of application that motivates this work, i.e. for simulation of low-viscosity fluids such as water in large vessels where the capillarity effects are negligible, a global slip condition with zero tangent stress is both appropriate and convenient; it does not require a complicated wetting model and simply allows the free surface to slide freely along the wetted boundary.

The slip boundary condition is a combination of Dirichlet and Neumann conditions, and can be expressed in the following way:

$$\begin{aligned} \mathbf{n} \cdot \mathbf{u} &= 0 \quad \text{on } \Gamma_{\text{slip}} \\ \mathbf{t} \cdot \boldsymbol{\sigma}(\mathbf{u}, p) \cdot \mathbf{n} &= 0 \quad \text{on } \Gamma_{\text{slip}} \\ \mathbf{b} \cdot \boldsymbol{\sigma}(\mathbf{u}, p) \cdot \mathbf{n} &= 0 \quad \text{on } \Gamma_{\text{slip}} \end{aligned} \tag{7}$$

where **n**, **t** and **b** are the normal, tangent, and (in three dimensions) bi-tangent vectors at the boundary. Alternately, Navier's slip condition is sometimes used to account for the wall friction:

$$\begin{aligned} \mathbf{n} \cdot \mathbf{u} &= 0 \quad \text{on } \Gamma_{\text{slip}} \\ \mathbf{t} \cdot \boldsymbol{\sigma}(\mathbf{u}, p) \cdot \mathbf{n} &= \beta \mathbf{t} \cdot \mathbf{u} \quad \text{on } \Gamma_{\text{slip}} \\ \mathbf{b} \cdot \boldsymbol{\sigma}(\mathbf{u}, p) \cdot \mathbf{n} &= \beta \mathbf{b} \cdot \mathbf{u} \quad \text{on } \Gamma_{\text{slip}} \end{aligned} \tag{8}$$

which prescribes a tangent stress proportional to the tangent velocity component with an empirical coefficient β. The implementation aspects differ depending on the complexity of the domain:

1. If the slip boundary coincides with a Cartesian co-ordinate plane, the implementation is trivial, with the equations corresponding to the normal component of velocity simply being dropped from the equation system.
2. If the slip boundary does not coincide with a Cartesian co-ordinate plane, the equations corresponding to the velocity components at the boundary are locally *aligned* with the normal-tangent-bi-tangent co-ordinate system, and the normal component of velocity is set to zero. This procedure is described by Engelman *et al.* [7], who also advocate the use of *consistent* normals for proper mass conservation.

In the second case, there is still a distinction between a slip boundary that is planar, with a uniform distribution of the normal vector, and a curved boundary, for which the normal vector varies depending on location. The non-uniform normal vector case is the subject of the discussion that follows. Our test application, described in more detail in Section 4, involves a circular cylindrical vessel shown in Figure 1, initially filled with fluid up to its half-height, placed in a uniform gravitational field and subsequently subjected to lateral oscillations.

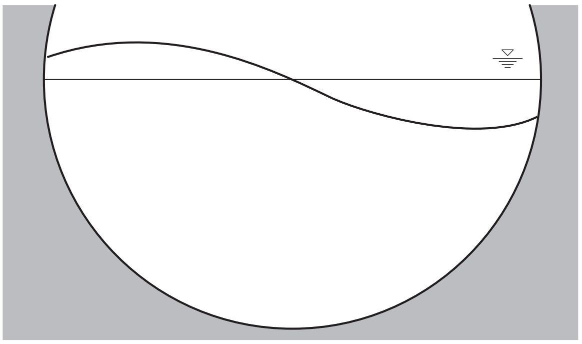

Figure 1. Circular vessel as an example of a simulation domain with curved domain boundaries.

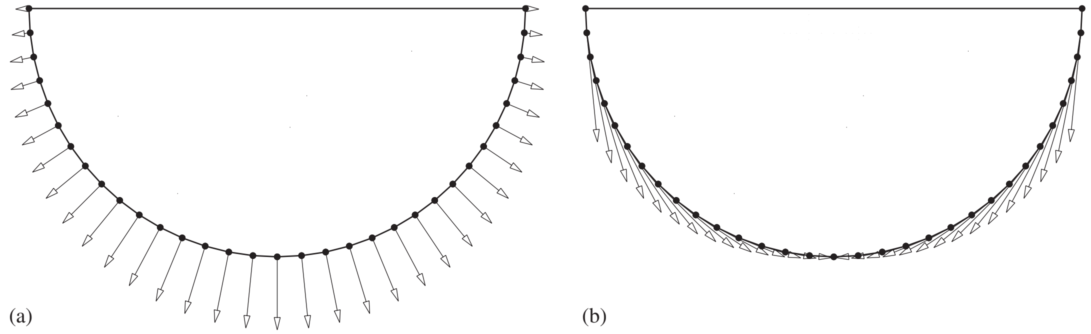

Figure 2. Nodal residual vectors in the discretized problem: (a) total nodal residual and (b) tangent component of residual (magnified).

Let us first consider the case of stationary fluid, subjected only to a constant uniform gravitational field $\mathbf{f}=\{0,-g\}$ (in two dimensions). The hydrostatic solution $\mathbf{u}=\mathbf{0}$, $p=-gy$ clearly satisfies the governing equations (1) and (2). The same solution is naturally expected to satisfy the discretized finite element form (6) when every one of the node-centred linear basis functions N_a is taken as the weighting function $\mathbf{w}^h$. This can be numerically verified at all interior nodes. At the boundary nodes, a non-zero momentum equation residual is obtained, as shown in Figure 2(a), and its normal component is dropped in accordance with the no-penetration boundary conditions. The problem arises due to the fact that, in the discrete case, the momentum equation residual at the curved boundary nodes also has a *non-negligible* component in the tangential direction; this component is shown in Figure 2(b), magnified by a factor of 1000 compared to Figure 2(a).

The reason for the non-zero tangential residual component becomes clear when one considers the difference between consistent normal directions at the nodes and the discrete residual directions, illustrated in Figure 3. In the figure, two boundary space–time edges P_n^i and P_n^j are adjacent to the node a. Consistent normal direction takes into account the boundary integrals indicated in the left subplot, with $\mathbf{n}_i$ and $\mathbf{n}_j$ assumed to be uniform along the corresponding edge, and N_a being the boundary trace of the basis function associated with node a. The

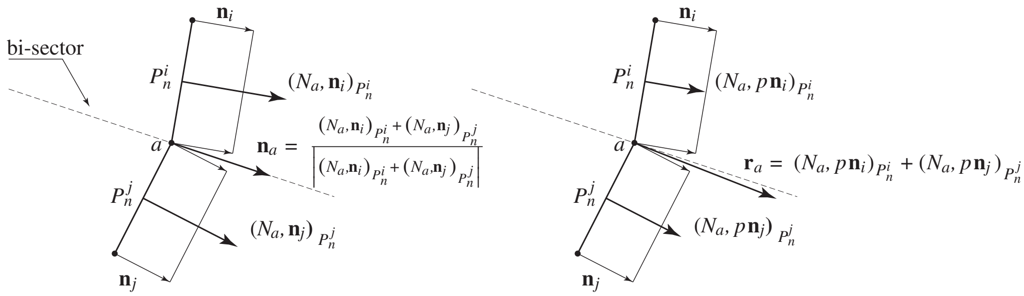

Figure 3. Difference between computed residual direction and the consistent normal direction at a node belonging to a curved boundary.

residual vector for the particular initial conditions considered here can be expressed as a sum of boundary integrals indicated in the right subplot; due to varying p (e.g. increasing linearly downward along each edge P_n^i and P_n^j) the resulting discrete residual will have a non-zero tangent component in the co-ordinate system defined by the consistent normal vector $\mathbf{n}_a$.

The non-zero residual signifies the fact that the stationary velocity field will not satisfy the discrete state equation, giving way to a non-zero velocity field that exhibits spurious recirculation regions, as shown in Plate 1(a), with a velocity magnitude range of $0 \leqslant |\mathbf{u}| \leqslant 3.40$. The Navier slip condition (8) can provide some resistance to that recirculation and improve the situation somewhat, as shown in Plate 1(b), with a velocity magnitude range of $0 \leqslant |\mathbf{u}| \leqslant 0.15$.

It has been observed that the recirculation regions persist in time-dependent simulations, when the tank is subjected to lateral oscillations. The slip-induced recirculation is not negligible when compared to the physical velocity field due to sloshing, and needs to be mitigated. It is apparent that a certain amount of tangent stress needs to be applied in the discrete problem to match the zero stress conditions of a continuum problem. In the stationary case, the necessary stress contribution at node a can be computed as

$$(N_a, \boldsymbol{h}^h)_{(P_n)_h} = [(N_a, (-gy)\mathbf{n}_i)_{P_n^i} + (N_a, (-gy)\mathbf{n}_j)_{P_n^j}] \cdot [\mathbf{I} - \mathbf{n}_a\mathbf{n}_a] \tag{9}$$

In other cases, the proper tangent stress correction is more difficult to determine. We resort here to the *BC-free* boundary condition, proposed by Papanastasiou *et al.* [18] and further investigated in References [19, 20]. This boundary condition, inadmissible in the continuum case but useful in the discrete case, extends the reach of the discretized governing equations to the boundary, and has been to date successfully applied at the traction-free, or outflow, boundaries. From the implementation point of view, the boundary integral in (6) is evaluated at node a using

$$(N_a, \boldsymbol{h}^h)_{(P_n)_h} = [(N_a, \boldsymbol{\sigma}(\mathbf{u}^h, p^h) \cdot \mathbf{n}_i)_{P_n^i} + (N_a, \boldsymbol{\sigma}(\mathbf{u}^h, p^h) \cdot \mathbf{n}_j)_{P_n^j}] \cdot [\mathbf{I} - \mathbf{n}_a\mathbf{n}_a] \tag{10}$$

i.e. the unknown velocity and pressure fields. As such, it produces contributions to both the left-hand-side matrix, and, if the initial condition is non-zero, to the residual vector. The normal component of this residual is dropped in the presence of no-penetration conditions, but the tangent component is retained, and counters precisely the tangent discrete stresses that lead to spurious recirculation. In the stationary case discussed above, the exact solution is

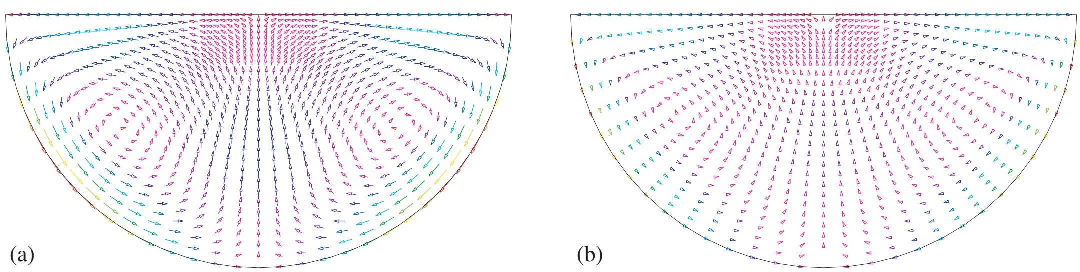

Plate 1. Spurious recirculating velocity fields: (a) equilibrium velocity filed $\beta = 0.0$ and (b) equilibrium velocity field $\beta = 0.1$.

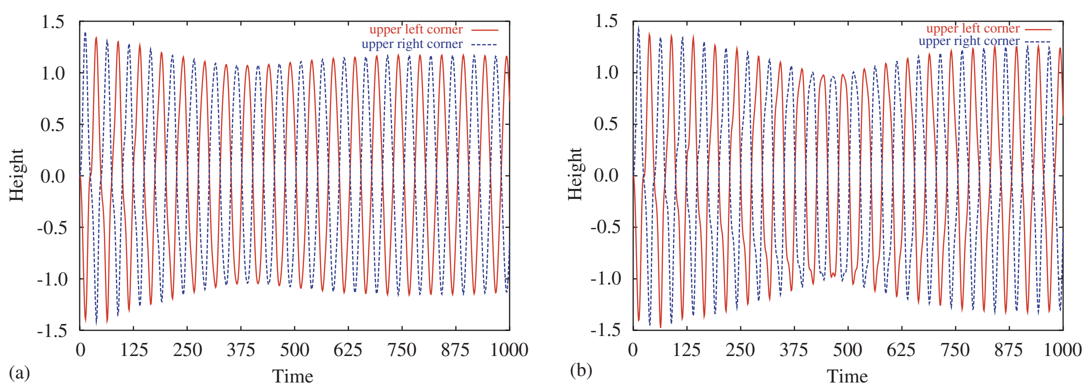

Plate 2. Circular tank: elevation history: (a) Navier slip $\beta = 0.1$ and (b) BC-free boundary condition.

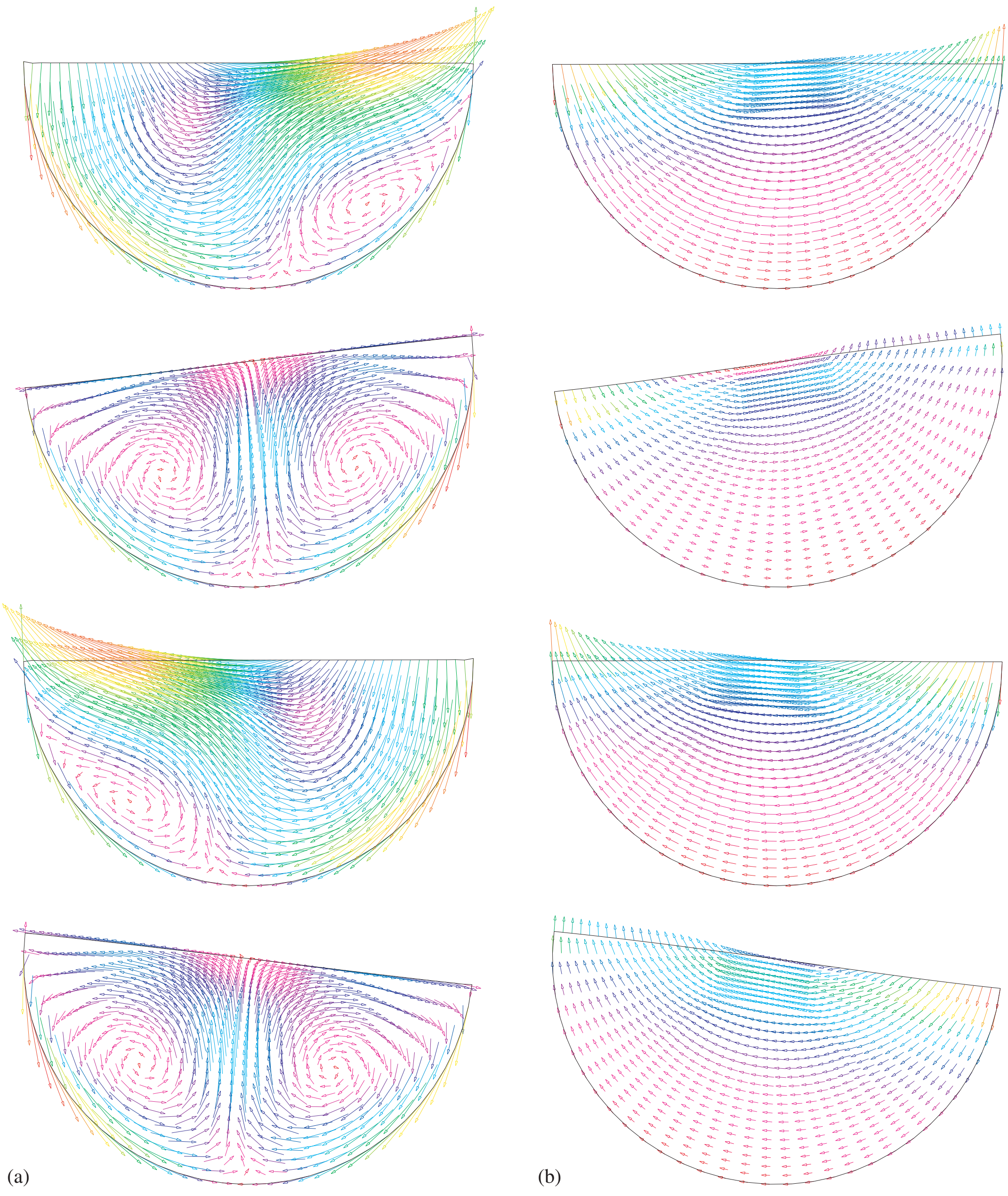

Plate 3. Circular tank: velocity field at $t = 955.0$, 967.5, 980.0 and 992.5 (top to bottom): (a) Navier slip $\beta = 0.1$ and (b) BC-free boundary condition.

also the solution of the discretized equations when BC-free condition is applied at the slip boundary. Further test in a non-stationary case is presented in the following section.

4. NUMERICAL EXAMPLE

The test problem, already outlined in Section 3, is a two-dimensional circular tank, with the initial domain shown in Figure 4(a). The tank is subjected to a downward gravitational acceleration of unit magnitude, and a sinusoidal horizontal acceleration with a magnitude of 0.1 and period of 16π. The fluid has unit density and a kinematic viscosity of 0.01, resulting in a Reynolds number of approximately 100, based on maximum sloshing velocity observed. The top boundary is the free surface, while the remaining boundary is subjected to three types of boundary conditions discussed so far: conventional slip condition (7), Navier slip condition (8) with $\beta = 0.1$, and BC-free boundary condition (10).

The finite element mesh consists of 768 quadrilateral elements and 1626 space–time nodes, as shown in Figure 4(b). The nodes at the slip boundary are allowed to move along the tank walls, i.e. along the line perpendicular to the consistent normal at those nodes, averaged between the initial and final position within each time step. The nodes at the free surface move along parametrized circular arcs using an extension of the method described in Reference [13]. An additional complication arises at the corner nodes corresponding to the edges of the free surface. At these two nodes, the residual equations are aligned using normals computed using the wetted surface edges only, and thus corresponding to directions shown in Figure 2(a). The use of consistent normal at these points would lead to a violation of the kinematic conditions.

The flow field is computed for 4000 time steps, with a time step size of 0.25, representing approximately 20 excitation periods. At each step, four non-linear iterations are used, resulting in four interspersed solutions of each of the systems involved (fluid, mesh, generalized elevation). A restarted GMRES solver with a Krylov space of 100 is used to solve the linearized equations.

The history of vertical displacement of the two upper corner nodes of the mesh is shown on Plate 2, for the case of Navier slip condition and BC-free condition. The conventional slip condition results in non-physical levels of recirculation and a spurious elevation rise around the symmetry line, and is not considered further. The Navier slip condition clearly damps some of the fine features of the sloshing, including the secondary waves clearly visible in

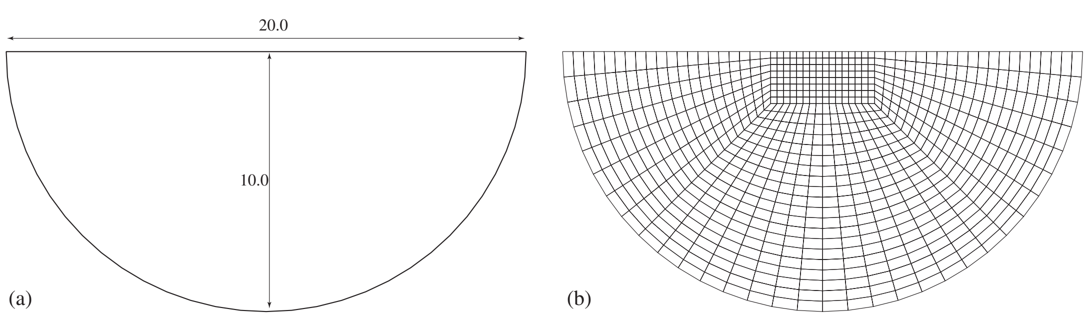

Figure 4. Circular tank: problem description: (a) computational domain and (b) finite element mesh.

Plate 2(b). As seen in the velocity field snapshots in Plate 3(b), the solution obtained using Navier slip condition is still exhibiting a degree of recirculation. On the other hand, the BC-free results in Plate 3(a) is free of recirculation.

5. CONCLUDING REMARKS

Numerical experiments indicate, and analysis confirms, that application of the slip boundary condition at curved boundaries is not straightforward. The tangent component of the discrete residual at a slip boundary is found not to vanish in a simple hydrostatic stationary flow field, and can induce a non-physical recirculating flow, also observed in the transient case. The Navier slip condition is found to provide some, but insufficient, degree of regularization. On the other hand, the BC-free boundary condition, extended to the slip boundary, is effective in maintaining both the stationary hydrostatic solution, and the expected non-recirculating transient solution.

ACKNOWLEDGEMENTS

This work was partially supported by the National Science Foundation under award CTS-ITR-0312764. The author gratefully acknowledges the computing resources made available by the National Partnership for Advanced Computational Infrastructure (NPACI). Additional computing resources were provided by the NSF MRI award EIA-0116289.

REFERENCES

1. Christodoulou KN, Scriven LE. The fluid mechanics of slide coating. *Journal of Fluid Mechanics* 1989; **208**: 321–354.
2. Christodoulou KN, Scriven LE. Discretization of free surface flows and other moving boundary problems. *Journal of Computational Physics* 1992; **99**:39–55.
3. Soulaïmani A, Fortin M, Dhatt G, Ouellet Y. Finite element simulation of two- and three-dimensional free surface flows. *Computer Methods in Applied Mechanics and Engineering* 1991; **86**:265–296.
4. Cairncross RA, Schunk PR, Baer TA, Rao RR, Sackinger PA. A finite element method for free surface flows of incompressible fluids in three dimensions. Part I. Boundary fitted mesh motion. *International Journal for Numerical Methods in Fluids* 2000; **33**:375–403.
5. Baer TA, Cairncross RA, Schunk PR, Rao R, Sackinger PA. A finite element method for free surface flows of incompressible fluids in three dimensions. Part I. Dynamic wetting lines. *International Journal for Numerical Methods in Fluids* 2000; **33**:405–427.
6. Kistler SF. Hydrodynamics of wetting. In *Wettability*, Berg JC (ed.). Dekker: New York, 1993; 311–429.
7. Engelman MS, Sani RL, Gresho PM. The implementation of normal and/or tangential boundary conditions in finite element codes for incompressible fluid flow. *International Journal for Numerical Methods in Fluids* 1982; **2**:225–238.
8. Tezduyar TE, Behr M, Liou J. A new strategy for finite element computations involving moving boundaries and interfaces—the deforming-spatial-domain/space–time procedure: I. The concept and the preliminary tests. *Computer Methods in Applied Mechanics and Engineering* 1992; **94**:339–351.
9. Tezduyar TE, Behr M, Mittal S, Liou J. A new strategy for finite element computations involving moving boundaries and interfaces—the deforming-spatial-domain/space–time procedure: II. Computation of free-surface flows, two-liquid flows, and flows with drifting cylinders. *Computer Methods in Applied Mechanics and Engineering* 1992; **94**:353–371.
10. Tezduyar TE, Aliabadi S, Behr M, Johnson A, Kalro V, Litke M. Flow simulation and high performance computing. *Computational Mechanics* 1996; **18**:397–412.
11. Behr M, Tezduyar TE. Finite element solution strategies for large-scale flow simulations. *Computer Methods in Applied Mechanics and Engineering* 1994; **112**:3–24.
12. Güler I, Behr M, Tezduyar TE. Parallel finite element computation of free-surface flows. *Computational Mechanics* 1999; **23**:117–123.

13. Behr M, Abraham F. Free surface flow simulations in the presence of inclined walls. *Computer Methods in Applied Mechanics and Engineering* 2002; **191**:5467–5483.
14. Behr M, Tezduyar TE. Shear-slip mesh update in 3D computation of complex flow problems with rotating mechanical components. *Computer Methods in Applied Mechanics and Engineering* 2001; **190**:3189–3200.
15. Stein K, Benney R, Kalro V, Tezduyar T, Leonard J, Accorsi M. Parachute fluid-structure interactions: 3-D computation. *Computer Methods in Applied Mechanics and Engineering* 2000; **190**:373–386.
16. Hirt CW, Amsden AA, Cook JL. An arbitrary Lagrangian Eulerian computing method for all flow speeds. *Journal of Computational Physics* 1974; **14**:227–253.
17. Johnson AA, Tezduyar TE. Mesh update strategies in parallel finite element computations of flow problems with moving boundaries and interfaces. *Computer Methods in Applied Mechanics and Engineering* 1994; **119**:73–94.
18. Papanastasiou TC, Malamataris N, Ellwood K. A new outflow boundary condition. *International Journal for Numerical Methods in Fluids* 1992; **14**:587–608.
19. Griffiths DF. The “no boundary condition” outflow boundary condition. *International Journal for Numerical Methods in Fluids* 1997; **24**:393–411.
20. Renardy M. Imposing “no” boundary condition at outflow: Why does it work?. *International Journal for Numerical Methods in Fluids* 1997; **24**:413–417.

